Journal of Solid State Chemistry **145,** 639–642 (1999)
Article ID jssc.1999.8267, available online at http://www.idealibrary.com on IDEAL®

Structure Determination of Ferromagnetic Perovskite $BiMnO_3$

T. Atou, H. Chiba,[1] K. Ohoyama, Y. Yamaguchi, and Y. Syono

Institute for Materials Research, Tohoku University, Katahira 2-1-1, Aoba-ku, Sendai 980-8577, Japan

Received November 25, 1998; accepted February 25, 1999

Structure of feromagnetic $BiMnO_3$ synthesized at high pressure has been determined by electron diffraction and neutron powder diffraction. This structure is related to a heavily distorted perovskite structure, having monoclinic symmetry, space group $C2$, with $a = 9.5323(6)$ Å, $b = 5.6064(3)$ Å, $C = 9.8535(7)$ Å, and $\beta = 110.667(5)^\circ$. The distortion is caused by a polarized Bi $6s^2$ lone pair. Every trivalent manganese cation reveals the Jahn–Teller distortion and ordering of a vacant $d_{x^2-y^2}$ orbital is suggested to play an important role for the ferromagnetism.
© 1999 Academic Press

Key Words: **magnetically ordered materials; chemical synthesis; crystal structure and symmetry; exchange and superexchange; neutron scattering.**

INTRODUCTION

Perovskite-type $BiMnO_3$ shows ferromagnetism (1–4). The observed magnetic moment at 5 K and 5 T reaches 3.6 μ_B, which is slightly smaller than that of the fully aligned spin value of 4 μ_B for Mn^{3+} (5, 6). Compared with $LaMnO_3$, which exhibits the A-type antiferromagnetism, this ferromagnetism should be noted because the ionic radii of trivalent bismuth and trivalent lanthanum are very close to each other (Bi^{3+}: 1.24 Å, La^{3+}: 1.22 Å, in 9-coordination).

$LaMnO_3$ has an orthorhombic $GdFeO_3$-type structure, and the mechanism of the A-type antiferromagnetism which shows parallel spin alignment within the c-plane and is antiparallel between adjacent c-layers is well explained by the orbital ordering of the vacant $d_{x^2-y^2}$ manganese orbital in the c-plane (7). On the other hand, $BiMnO_3$ has a triclinically distorted perovskite structure with $a = c = 3.935$ Å, $b = 3.989$ Å, $\alpha = \gamma = 91.4^\circ$, $\beta = 91.0^\circ$, taking the unit cell on the basis of the perovskite lattice (5). This lower symmetry structure has been explained by a highly polarized $6s^2$ character of Bi^{3+} (1). To clarify the origin of the ferromagnetism in $BiMnO_3$, an accurate structural analysis is indispensable to determine the atomic parameters which have not been determined yet.

[1]Present address: Yamagata Fujitsu Ltd., Higashine-Ko 5400-2, Higashine 999-3701, Japan.

We have reported superlattice spots observed in electron diffraction patterns of $BiMnO_3$ and proposed a larger unit cell of $a = 9.54$ Å, $b = 5.61$ Å, $c = 9.86$ Å, and $\beta = 110.7^\circ$ (8). In this unit cell, extinction satisfies a C base-centered lattice. However, an accurate crystal structure could not be determined from Rietveld analysis of an X-ray powder diffraction because of weak scattering power from oxide ions. Also, it is very difficult to obtain a single crystal sample, because $BiMnO_3$ can be obtainable only under high pressure.

In this paper, we have measured a high resolution neutron powder diffraction pattern and successfully analyzed its structure by Rietveld refinement. The origin of the ferromagnetism is discussed in comparison with antiferromagnetic $LaMnO_3$.

EXPERIMENTS AND DATA ANALYSIS

The synthesis of the poly crystalline sample of $BiMnO_3$ was carried out by a high-pressure technique. The mixture of Bi_2O_3 and Mn_2O_3 with a 1:1 ratio was encased in a gold capsule (∅, 2.5 mm; height; 2.5 mm) and placed in a tubular graphite heater, which was embedded in a 8-mm pyrophillite cube and subjected to high pressure by means of a DIA-6 type cubic press with 6 mm anvils. A complete reaction was obtained by keeping the mixture at 700°C and 6 GPa for 3 h. To obtain a sufficient amount (~100 mg) of $BiMnO_3$ for neutron diffraction study, several runs were repeated.

Neutron powder diffraction experiments were carried out at room temperature using HERMES (high efficiency high resolution measurements) installed at JRR-3M of the Japan Atomic Energy Research Institute. In the HERMES detector bank, 150 ^{3}He counters were placed at every 1° of diffraction angle, being able to perform a rapid and high resolution neutron diffraction experiment. The detail of this diffractometer has been published elsewhere (9). The sample was contained in a vanadium can with 5 mm in diameter and 5 mm in height.

Intensity data were taken with thermal neutron radiation at $\lambda = 1.8196$ Å (from a Ge 331 monochromator) in the 2θ range from 3° to 153° in step size 0.1°. Twenty-two minutes for every step are needed to collect approximately 1000

0022-4596/99 $30.00
Copyright © 1999 by Academic Press
All rights of reproduction in any form reserved.

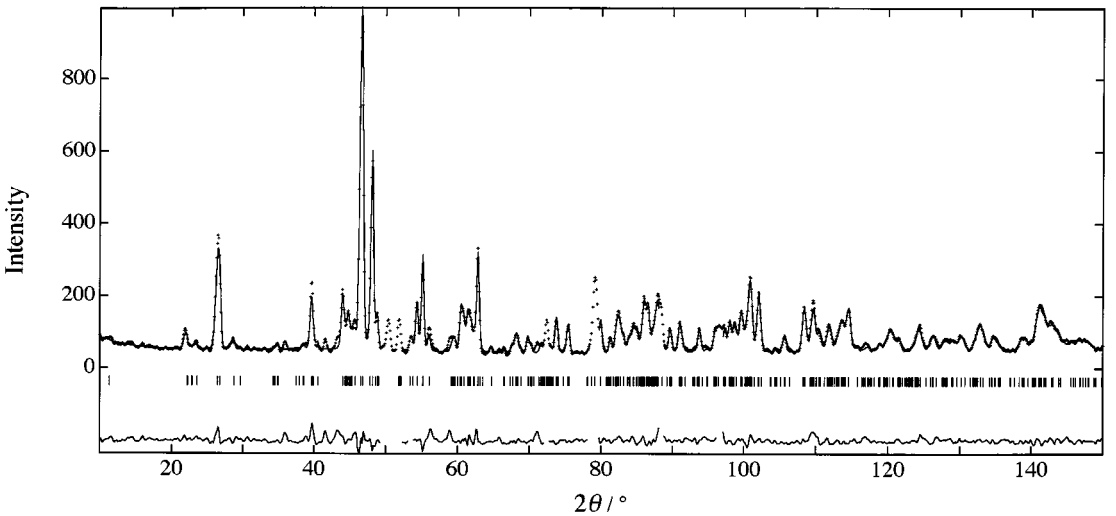

FIG. 1. The observed (dots) and calculated (line) profile of $BiMnO_3$ after the final refinement.

counts for the strongest diffraction line. Intensity data from 10° to 150° were used in the structural refinements using Rietveld analysis code RIETAN-97 β (10). Since this sample contained a small amount of impurity phases ($Bi_2(CO_3)O_2$ and unknown phase), some parts of the data were eliminated for the analysis. The neutron scattering lengths used for the refinement were $b^{Bi} = 8.531$, $b^{Mn} = -3.730$, and $b^{O} = 5.803$ in units of 10^{-15} m.

From the observation of the electron diffraction, as reported previously, possible space groups were limited to $C2$ (No. 5), Cm (No. 7), and $C2/m$ (No. 12) (8). Since $C2$ (No. 5) resulted in the best fit among them, the space group was assumed to be $C2$ (No. 5). The origin was set on the manganese atom. Parameters were refined in the following order: (1) background, scale, and profile parameters; (2) positional parameters; (3) we refined all parameters including isotropic-thermal parameters.

Figure 1 shows the neutron diffraction pattern of $BiMnO_3$ at room temperature. The dots and lines in the upper part of the figure correspond to the observed and calculated intensity, respectively. The deviation of the former from the latter is also shown in the figure. Good agreement between the observed and calculated intensity was obtained. The reliability factors were $R_{wp} = 8.07\%$, $R_p = 5.93\%$, $R_e = 10.46\%$, $(S = R_{wp}/R_e = 0.7710)$, $R_I = 2.49\%$, and $R_F = 1.56\%$. The refined cell parameters were $a = 9.5323(6)$ Å, $b = 5.6064(3)$ Å, $c = 9.8535(7)$ Å, and $\beta = 110.667(5)°$. The final structural parameters are summarized in Table 1. Selected interatomic distances and bond angles are given in Table 2.

DISCUSSION

Figure 2 shows a schematic illustration of the refined crystal structure of $BiMnO_3$. This structure is a heavily distorted perovskite structure. Influence of the Bi $6s^2$ lone pair is most clearly seen in a part of the structure projected along [301], which corresponds to the closest packing plane consisting of a bismuth cation and an oxide anion (Fig. 3). The bismuth cation is shifted from the center of the hexagon of the oxide anion due to the polarized lone pair of the bismuth cation, resulting in a lowering of the symmetry of the whole structure. Assuming that the coordination number of the bismuth cation is 9, mean interatomic distances are 2.69 and 2.63 Å for the Bi1 and Bi2 sites, respectively. These values agree well with the summation of ionic radii (1.24 Å (Bi^{3+}) + 1.40 Å (O^{2-}) = 2.64 Å), indicating the validity of the refinement (11).

TABLE 1
Refined Stuctural Parameters of $BiMnO_3$[a]

Atom	Site	x	y	z	B(Å^2)
O1	4c	0.100(2)	0.015(5)	0.838(1)	0.9(2)
O2	4c	0.400(2)	0.169(5)	0.672(1)	0.4(2)
O3	4c	0.149(2)	0.405(4)	0.630(1)	0.6(2)
O4	4c	0.346(2)	0.363(5)	0.415(2)	0.7(2)
O5	4c	0.365(2)	0.276(5)	0.915(2)	0.9(2)
O6	4c	0.144(2)	0.257(4)	0.106(2)	1.1(2)
Bil	4c	0.135(1)	0.037(4)	0.372(1)	0.5(2)
Bi2	4c	0.359(1)	0.100(4)	0.115(1)	0.7(2)
Mn1	2a[b]	0	0	0	0.5(3)
Mn2	4c	0.254(3)	0.062(8)	0.757(3)	0.2(2)
Mn3	2b	0.5	0.096(5)	0.5	0.2(3)

Note. Occupancies for all sites were assumed to be 1.0. $R_{wp} = 8.07\%$, $R_p = 5.93\%$, $R_I = 2.49\%$, and $R_F = 1.56\%$.

[a]Space group: $C2$ (No. 5), $a = 9.5323(6)$ Å, $b = 5.6064(3)$ Å, $c = 9.8536(7)$ Å, and $\beta = 110.667(5)°$.

[b]Mn1 site was fixed at the origin.

TABLE 2
Selected Interatomic Distances and Bond Angles of $BiMnO_3$ in Å and Degree, Respectively

Bi1–O1	2.45(2)	O5–Mn1–O5	90.3(13)
Bi1–O2	2.11(2)	O6–Mn1–O6	88.5(12)
Bi1–O2	3.23(2)	O6–Mn1–O5	90.7(6)
Bi1–O3	2.20(2)	O6–Mn1–O5	176.0(7)
Bi1–O4	2.26(2) × 2	O1–Mn1–O1	175.5(15)
Bi1–O4	3.09(2)	O1–Mn1–O6	87.5(7)
Bi1–O5	3.18(2)	O1–Mn1–O6	89.3(7)
Bi1–O6	2.92(2)	O1–Mn1–O5	86.8(8)
		O1–Mn1–O5	96.4(8)
Bi2–O1	2.38(2)		
Bi2–O1	3.00(2)	O5–Mn2–O3	85.9(14)
Bi2–O2	2.54(2)	O6–Mn2–O5	89.5(11)
Bi2–O3	2.76(2)	O4–Mn2–O3	91.1(10)
Bi2–O5	2.23(2)	O6–Mn2–O4	93.7(15)
Bi2–O5	2.74(2)	O2–Mn2–O1	169.7(21)
Bi2–O5	2.92(2)	O5–Mn2–O4	173.4(21)
Bi2–O6	2.20(2)	O6–Mn2–O3	174.8(17)
Bi2–O6	2.90(2)	O6–Mn2–O1	82.7(11)
		O5–Mn2–O1	91.9(15)
Mn1–O1	2.13(1) × 2	O3–Mn2–O1	95.0(14)
Mn1–O5	1.78(2) × 2	O4–Mn2–O1	94.2(16)
Mn1–O6	2.01(2) × 2	O5–Mn2–O2	83.3(15)
		O6–Mn2–O2	106.2(15)
Mn2–O1	1.93(3)	O4–Mn2–O2	90.3(15)
Mn2–O2	1.95(3)	O3–Mn2–O2	75.7(11)
Mn2–O3	2.32(3)		
Mn2–O4	1.97(4)	O4–Mn3–O4	86.6(10)
Mn2–O5	1.96(4)	O3–Mn3–O3	110.4(13)
Mn2–O6	2.18(3)	O4–Mn3–O3	83.0(6)
		O4–Mn3–O3	162.3(8)
Mn3–O2	2.26(1) × 2	O2–Mn3–O2	159.0(12)
Mn3–O3	1.87(2) × 2	O2–Mn3–O4	89.6(8)
Mn3–O4	2.06(2) × 2	O2–Mn3–O4	75.1(7)
		O2–Mn3–O3	90.5(5)
		O2–Mn3–O3	101.5(6)

Figure 4 shows the coordination environment around the manganese cations. Although the coordination polyhedra are fairly distorted from the regular one, they still form MnO_6 octohedra for all manganese sites. Such a distortion

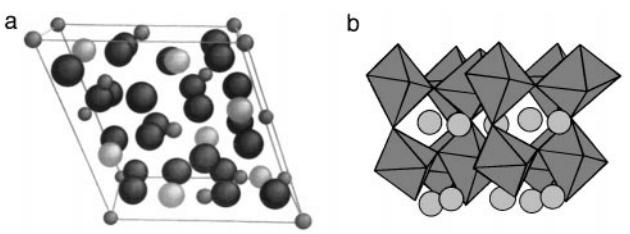

FIG. 2. Schematic illustrations of crystal structure of $BiMnO_3$. (a) Unit cell view: large, O^{2-}; middle, Bi^{3+}; small, Mn^{3+}. (b) A part of the crystal structure is shown on the basis of the perovskite unit. MnO_6 octahedra and bismuth cations are represented.

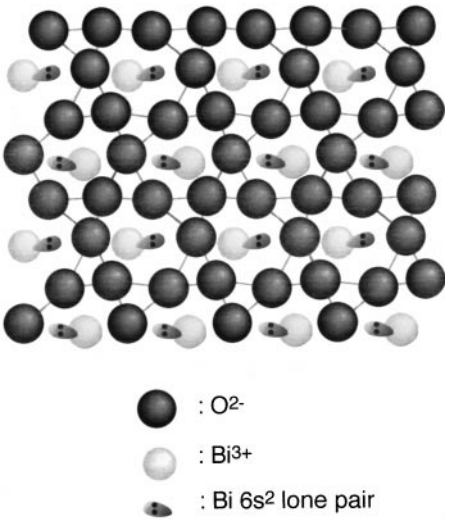

FIG. 3. The closest packing plane which consists of bismuth cations and oxide anions. Polarized Bi $6s^2$ lone pairs are shown schematically.

of polyhedra is sometimes seen in a Mn^{3+} compound like Mn_2O_3 with the C-type rare-earth oxide structure. Interatomic distances and bond angles of these MnO_6 octahedra are summarized in Table 2. The mean Mn–O distance is 1.97, 2.05, and 2.06 Å for the Mn1, Mn2, and Mn3 sites, respectively. These values are consistent with the summation of the ionic radii of Mn^{3+} and O^{2-} (2.03 Å) (11). It is noted that these octahedra reveal uni-axial elongation. The elongation is about $12 \sim 15\%$ of the mean Mn–O distance of the in-plane Mn–O distances. This should be explained by the Jahn–Teller distortion of the trivalent manganese cation with a d^4 electronic configuration. This elongation suggests that the degenerated e_g orbital splits into $d_{x^2-y^2}$ and d_{z^2} orbitals and the e_g electron occupies a d_{z^2} orbital for every manganese cation.

Goodenough has provided explanation for the antiferromagnetism of $LaMnO_3$ from a viewpoint of so-called

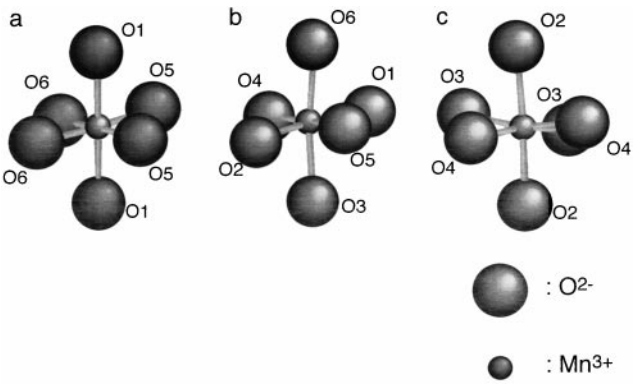

FIG. 4. MnO_6 octahedra are shown for (a) Mn1, (b) Mn2, and (c) Mn3 sites.

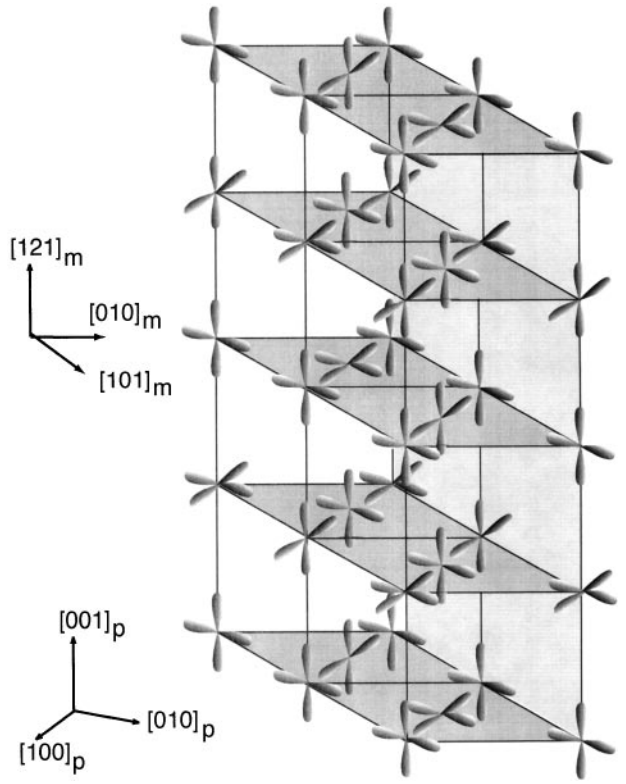

FIG. 5. The ordering of the vacant $d_{x^2-y^2}$ orbital of Mn^{3+} is illustrated for $BiMnO_3$. This unit can be regarded as a retaken unit cell with $2\sqrt{2}a_p \times \sqrt{2}a_p \times 4a_p$, $z = 16$, in which a_p represents a cell constant of a primitive perovskite unit cell. Directions for the original (monoclinic) unit cell and the primitive perovskite cell are also shown.

"orbital ordering," in which the ordering of vacant orbitals plays an important role in the superexchange interaction (7). According to Goodenough's idea, ferromagnetic $BiMnO_3$ might also reveal an orbital ordering like $LaMnO_3$. Figure 5 represents a schematic illustration of a vacant $d_{x^2-y^2}$ orbital for $BiMnO_3$, presumed from the direction of the Jahn–Teller distortion. Although the orbital configurations, which are favourable for the antiferromagnetic interaction, are partially seen, two thirds of the Mn–O–Mn orbital configurations favourable for ferromagnetic interaction via superexchange interaction are rather uniformly distributed. For every manganese cation, four ferromagnetic and two antiferromagnetic interactions can be seen. We believe that the ferromagnetic interaction overcomes the antiferromagnetic interaction below the critical temperature, and consequently, the ferromagnetism of $BiMnO_3$ appears. A slightly reduced magnetic moment from a fully aligned spin value and its gradual increase at high field (5, 6) may be attributable to partial antiparallel spins. Neutron diffraction study below T_c is underway to clarify the nature of the magetic property.

$BiMnO_3$ is an insulator. This is probably concerned with Mn–O–Mn bond angles which are fairly apart from 180° (distributed between 160° and 140°). When a bismuth cation is partly substituted by a strontium cation to dope carriers, the electrical resistivity decreases, but still remains a thermally activated behavior (5, 6). Also, the ferromagnetism rapidly disappears. These indicate that the double exchange mechanism does not work in this system and the ferromagnetism appears via superexchange interaction in the orbital ordered state as mentioned above.

ACKNOWLEDGMENTS

The authors thank Drs. H. Faquir and M. Kikuchi for useful discussion and Mr. K. Netmoto for assistance in the course of the neutron diffraction experiment. This research was partially supported by a grant-in-aid, for scientific research by the Ministry of Education, Science and Culture, Japan.

REFERENCES

1. F. Sugawara, S. Iida, Y. Syono, and S. Akimoto, *J. Phys. Soc. Jpn.* **25,** 1553 (1968).
2. F. Sugawara, S. Iida, Y. Syono, and S. Akimoto, *J. Phys. Soc. Jpn.* **20,** 1529 (1965).
3. V. A. Bokov, I. E. Myl'nikova, S. A. Kinzhaev, M. F. Bryzhina, and N. A. Grigoryan, *Soviet Phys.-Solid State Chem.* **1,** 409 (1970).
4. I. O. Troyanchuk, N. Y. Kasper, O. S. Mantytskaya, and S. N. Pastushonok, *J. Exp. Theor. Phys.* **78,** 212 (1994).
5. H. Chiba, T. Atou, and Y. Syono, *J. Solid State Chem.* **132,** 139 (1997).
6. Y. Syono, H. Chiba, and T. Atou, *J. Mag. Soc. Jpn.* **22,** 52 (1998).
7. J. B. Goodenough, *Phys. Rev.* **100,** 564 (1955).
8. H. Chiba, T. Atou, and Y. Syono, *Solid State Ionics* **108,** 193 (1998).
9. K. Ohoyama, T. Kanouchi, K. Nemoto, M. Ohashi, T. Kajitani, and Y. Yamaguchi, *Jpn. J. Appl. Phys.* **37,** 3319 (1998). [Brief information is also available on the internet at http://monmon.imr.tohoku.ac.jp/HERMES.html]
10. F. Izumi, "*The Rietveld Method*" (R. A. Young, Ed.), Chap. 13. Oxford University Press, Oxford, 1993.
11. R. D. Shannon and C. T. Prewitt, *Acta Cryst.* **B 25,** 925 (1969).